

# Machine Learning on Greenest Pixels for Crop Mapping

Ziheng Sun, Liping Di, Hui Fang

Center for Spatial Information Science and Systems

George Mason University

**Abstract:** Crop fields are full of uncertainties due to the complexity of the environment, seeds, climate, market, and farmers. It is a common phenomenon that the crops in neighbor fields are in different growing stages, e.g., the corns in one field are already dented but just emerged in another neighbor field. The phenomenon results in remote sensing images that are non-ideal for producing crop maps as the crops are in different phases across the fields. For instance, July is the best month for monitoring soybeans but bad for winter wheat. Most of the wheat fields are already harvested in July and appear like fallow fields on satellite images. This paper proposes a customized classification approach based on greenest pixels (GP) to enhance the quality of the satellite images for mapping. The greenest pixels are got by calculating the largest NDVI (Normalized Difference Vegetation Index) values of every pixel from all the captured images each year. In the process, we filtered the bad quality pixels like clouds, ice, snow, shadow, etc. A filtering step is added to distinguish the non-vegetation and vegetation pixels first. The overall workflow uses state-of-art remote sensing classification techniques. Machine learning (ML) algorithms like KNN, Gaussian Naïve Bayes, Decision Tree, AdaBoost, Random Forest, SVM, and Neural Networks were used simultaneously to evaluate the approach. The study area is located on the farms of Nebraska. They used satellite imagery includes Landsat 8 surface reflectance products. The ground truth data comes from field surveys, roadside samples, and USDA (United States Department of Agriculture) crop maps. Google Earth Engine was used to accelerate the data preprocessing. We tested all the ML models on two sets of experiments: GP and non-GP. In each set, the training has only one-year data (2013) and the testing uses the rest years (2014-2018). The results show that the proposed GP-based approach can significantly improve the classification precision by ~20% (from ~70% to 85%) on average. This research proves that greenest pixels have large potential and should be considered as the major input data in the crop mappings in the future.

**Keywords:** greenest pixel; machine learning; land cover; remote sensing; image classification.

## 1. Introduction

Remote sensing plays a big role in agriculture monitoring today. Satellites, drones, airplanes take thousands of images about farm fields every day [1-5]. A lot of useful information is hidden in these images. Via these images, people can monitor the recent progress of crops, analyze the impacts of disasters, and study the vegetation phenology [6,7]. To reveal the contained information and make them easy to read, scientists produce many thematic maps regarding various application purposes. For instance, agricultural drought maps are generated to guide the irrigation [7-9]. Vegetation health maps are derived to guide the use of chemicals to boost the yields and protect the crops from disease, weeds, infestation, etc [10,11]. The crop distribution map is normally produced annually to show the crop types growing on the fields in that year [12]. Due to the low cost and high availability of remote sensing images, remote sensing image classification is now the major method to produce in-time and large-scale agricultural thematic maps [13].

The common classification techniques can be categorized into two types: unsupervised classification and supervised classification [14]. Thematic classification tasks like crop distribution mapping should use supervised classification [15]. To assist the supervised classification on a large scale, a tremendous amount

43 of ground truth data points is required to train the models and validate the results. However, the cost of  
 44 collecting ground truth data is much higher than remote sensing data at present, which is one of the major  
 45 bottleneck problems in crop mapping. USDA (United States Department of Agriculture) has devoted long-  
 46 term efforts to survey the crop fields every year and collected a complete systematic set of ground  
 47 measurements by their field offices. Use that data, USDA NASS (National Agricultural Statistics Service)  
 48 produces Cropland Data Layer (CDL), annual crop maps of continental United States at the resolution of  
 49 30 meters by classifying the imagery of Landsat and some other satellites [16,17]. See5, a renowned decision  
 50 tree software, is used to carry out the classification for CDL [18]. CDL owns a very high accuracy that  
 51 ranges from 82% to 95%. Some large farm areas could even reach to 97% [1,17]. Recent new research  
 52 shows that applying new supervised classification could improve the accuracy further while reducing the  
 53 dependence on ground truth data by creating reusable classification models. Many papers highlighted ML  
 54 models could increase the accuracy and reusability significantly [12,19-22].

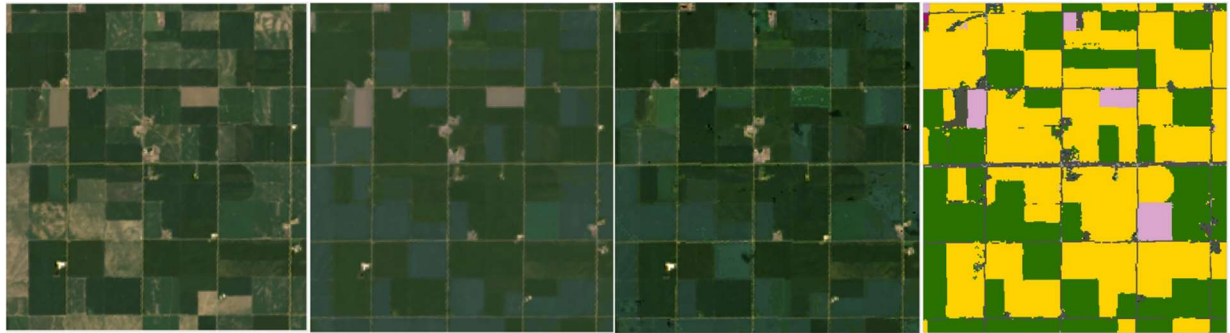


57 Figure 1. The raw true-color Landsat images (top row from left to right: 2018-04-05, 2018-05-07, 2018-  
 58 05-23, 2018-06-08; bottom row from left to right: 2018-07-10, 2018-08-11, 2018-09-12, 2018-11-15)

59 Besides ground data, the selection of remote sensing images is another challenge in improving map  
 60 quality. The phenology of various crop types has huge differences, which results in that not all the remote  
 61 sensing images are suitable for classification. Fig. 1 shows the Landsat true-color images [23] of the same  
 62 area on different days in 2018. This area is located at the heart of Nebraska, a major corn/soybean state in  
 63 the nation [6]. The image of April 5 has no green fields, indicating that no crops are planted or not emerging  
 64 yet. This image doesn't contain any information on crops. In the images on May 7 and 23, several alfalfa  
 65 fields become green as they are planted early and grow fast. In the June 8 image, cornfields start to green  
 66 up while some of the alfalfa fields have been cut for the first time (alfalfa field turns light green). In the  
 67 July 10 image, corn has entered the black layer stage, while soybeans also become visible. On August 11,  
 68 corn and soybean have reached full maturity and are ready for harvesting. Alfalfa was harvested for another  
 69 time and turns light green again. On September 12, most corn fields were harvested, and alfalfa grows up  
 70 again. In the November 15 image, all the fields returned to idle like the first image of April 5. The first four  
 71 images and the last two images are not suitable to identify corn and soybeans but good for recognizing  
 72 alfalfa and field ridges. The revisiting period of the same place of every satellite differs every year and so  
 73 do the crop phenological milestones, which are greatly influenced by the farmer's decisions and

74 environment. Due to these uncertainties, searching and selecting suitable remote sensing images suitable  
75 for classification takes a lot of manual efforts and is labor-intensive to scale up to a large scale and charges  
76 a higher cost on consumers to get high-resolution crop maps.

77 To address these challenges, this paper proposes a novel approach using greenest images and machine  
78 learning (ML) models in producing crop maps. Greenest images are calculated by extracting the greenest  
79 pixels from all the captured images in one year. The greenness is measured by NDVI (normalized difference  
80 vegetation index) [24]. In other words, the pixels with the highest NDVI values are considered as the  
81 greenest pixels. The pixels in the greenest image should all be the greenest of the year. Classic ML models  
82 are created to take the greenest images as inputs and output a thematic map of crop types. The resulting  
83 map is a raster image, in which the pixel values correspond to crop categories. For instance, 1 represents  
84 corn, and 5 represents soybean. Fig. 2 shows a comparison between original true-color Landsat images,  
85 greenest images, and thematic crop maps in 2018. It is clear that all the crop fields in the greenest image  
86 are green and covered by crops, unlike the original Landsat images always including some idle fields. The  
87 thematic crop map renders different land cover types with various colors for better readability. In the CDL  
88 hierarchy, there are more than 100 crop types.



89  
90 Figure 2. From left to right: 07-10-2018, 08-11-2018, Greenest Image of 2018 and CDL of 2018 (yellow:  
91 corn; green: soybean; pink: alfalfa; black: roads)

92 In this work, a new workflow streamlining the preparation and feeding of greenest images into ML  
93 models is built and experimented. The workflow translates the ML model results to crop maps which are  
94 ready for stakeholders to use. The whole workflow involves dozens of tools, resources, and libraries, and  
95 requires better management to improve efficiency. The study area chooses a farm located in the heart of  
96 Nebraska and the data sources are Landsat 8. The images are preprocessed to become consumable arrays  
97 in ML models. Classic ML models including KNN, Gaussian Naïve Bayes, AdaBoost, Decision Tree, SVM,  
98 Random Forest, and Multilayer Perceptron, are all tested to validate the superiority of the GP approach.  
99 The ML models extract the high-level features from the images to identify and recognize the crops. Random  
100 Forest and Multilayer Perceptron have been proven to be more accurate and generalizable than the other  
101 classification models regarding both major and minor crops. The trained models are proven to be reusable  
102 on future images to automatically generate crop maps without needs for collecting new ground truth or  
103 retraining.

104 The remainder of this paper is organized as follows. Section 2 gives the background and motivation of  
105 this work. Section 3 introduces the study area and the used datasets. In Section 4, deep learning is briefly  
106 introduced as the existing state-of-art work. Section 5 describes the proposed GP-based approach. The  
107 experiment and results are described in Section 6 and Section 7 evaluates the performance of the approach  
108 by comparing it to other existing approaches. Section 8 concludes the work and gives the work items in the  
109 future.

## 110 2. Background

### 111 2.1 The Role of Farm Maps in Decision Making

112 Smallholder farmers are sitting on the front line of agricultural decision making. They are farmers that  
113 have more than half of farm work done by family members, cooperative members or neighbors. Decision  
114 making is central to farm management. Each decision has an impact on the farm and the farm household.  
115 Even deciding to do nothing is a decision and has an impact. The more a farmer is aware of the decision-  
116 making processes that affect farm and household, the more sustainable the farm will be and the more likely  
117 it will be profitable and sustainable. Farm decisions are closely tied to decisions made in the household.

118 The most characteristic aspects of farming operations are the changes that continuously occur, and the  
119 lack of knowledge concerning conditions that affect farm businesses. Market prices, the knowledge of  
120 smallholder farmers, techniques, weather, health, and governmental arrangements change all the time.  
121 Throughout the agriculture history, farmers had to make decisions based only upon observation and  
122 recollection. Both sources are not precise, but it was the best data available [25].

123 As scientific methods were introduced, farmers could employ research-derived recommendations to  
124 improve production efficiency. Digital technologies are changing the routine of farmers in making their  
125 daily decisions. The evolution of those capabilities offers significant benefits for farmers and the entire food  
126 supply industry<sup>1</sup>. Farmers have long desired to link measures of outcomes and management actions in  
127 farming. Advanced technologies like remote sensing and sensor web give farmers the ability to routinely  
128 capture and exploit data to get their desired information. The crop distribution map is an important member  
129 of the desired data. Farmers need to get an overview of what other farmers are growing and how many acres  
130 are covered by the same crop over the entire region. The information would greatly help them make an  
131 economic-wise choice on choosing crops to increase their household income.

132 Other thematic farm maps will identify areas on the farm that are vulnerable to water contamination,  
133 and practices that may contribute to water pollution. The base map of the farm should show all farm fields,  
134 the farmstead and barnyard area, associated use areas, wetlands, and forests. Another value of a farm map  
135 is for future planning or to best utilize their property. A farm map can also identify soil types and other  
136 characteristics, such as slope, that can be useful in making decisions like grazing plans and crop rotations.  
137 A map can be helpful when selecting compost or manure storage areas. It can also play an important role  
138 in emergency planning or responding.<sup>2</sup>

## 139 2.2 Challenges and Opportunities

140 Cutting-edge techniques have been utilized in farmland mapping for a long time. Satellite remote  
141 sensing is a low cost and reliable way and has been used in the land survey for many years. The remote  
142 sensing data is mostly available free and easy to access via web services. Recently, NASA and NOAA have  
143 worked with giant tech companies to migrate their big datasets to the commercial clouds that have better  
144 scalability and stability for data retrieval. Cloud-native services provide big data processing capabilities  
145 that are never seen before, such as Google Earth Engine (GEE). This latest development in satellites and  
146 cloud computing has made it convenient to produce agriculture maps in an efficient and economical manner.  
147 With the development of intelligent farming devices such as autonomous tractors, remotely monitoring  
148 farmland and operating devices to farm efficiently is a big wish of the humankind for the next generation  
149 of agriculture. Remote sensing is a key component playing the eye-in-the-sky role in this ambitious vision.  
150 It provides critical information about the crops in the field and transfers the information to decision making  
151 parties to develop and apply solutions or operations.

## 152 3. Data and Study Area

### 153 3.1 Study Area

154 The study area is within the central region of Nebraska, one of the major corn-belt states. The crops

---

<sup>1</sup> <https://farmdocdaily.illinois.edu/2020/03/evidence-data-and-farmer-decision-making.html>

<sup>2</sup> <https://njaes.rutgers.edu/fs1189/>

155 include soybeans, and corn, alfalfa, and some winter wheat. In 2018, the ten leading commodities for cash  
156 receipts in Nebraska are cattle and calves, corn, soybeans, hogs, wheat, dairy products (milk), misc. crops,  
157 hay, chicken eggs, and potatoes. Among them, corn is Nebraska's most important crop, with much of it  
158 going to feed cattle and hogs. The state had 45,900 farms and ranches during 2018 and the average operation  
159 consisted of 980 acres (397 ha). The landscape of Nebraska has a 4,584 feet elevation difference, and the  
160 average annual precipitation decreases by one inch every 25 miles from east to west. The agricultural  
161 industry in Nebraska shows a diverse change from one side to the other.

### 162 3.2 Data Sources

#### 163 (1) Landsat 8

164 Landsat 8 is the latest in-orbit satellite of the Landsat program and was launched in 2013 [23]. The  
165 satellite has two major sensors onboard: Operational Land Images (OLI) and the Thermal Infrared Sensor  
166 (TIRS). It circles the Earth every 99 minutes and has a 16-day repeat cycle for any location on the Earth. It  
167 acquires about 740 scenes a day on the Worldwide Reference System-2 (WRS-2) path/row system. The  
168 mostly used bands come from OLI include nine bands at 30-meter resolution. The band range is kept  
169 consistent with the bands of old TM/ETM sensors carried by previous Landsat satellites.

#### 170 (2) Cropland Data Layer (CDL)

171 CDL is a georeferenced raster crop map of the U.S. at a spatial resolution of 30 meters. It is derived by  
172 classifying satellite imagery using reliable classification algorithms and the massive amount of ground truth  
173 data collected by the United States Department of Agriculture (USDA) National Agricultural Statistics  
174 Service (NASS). It is released yearly and normally published in next February. The accuracy in the crop  
175 fields ranges from 85% to 95%. The data is available for the lower 48 states since 2008. Before that, only  
176 a few states are available. Due to its high quality, it has been used in many major researches related to  
177 agriculture by both academia and industries.

#### 178 (3) Roadside Survey

179 The ground truth data of USDA, Common Land Unit (CLU), is not in the public domain [26]. To  
180 validate our classification results, we collected ground observations via very high-resolution images, field  
181 surveys, and road trips. Many people in the U.S. enjoy identifying and observing farms and farm activity  
182 while on a road trip. We made several trips to Nebraska and drive a big circle from Omaha to Ogallala and  
183 drive back via Norfolk. The trips occurred in July and we took 1,095 photo samples in total showing the  
184 growing crops. We processed all the photos and translate them into a collection of ground truth polygons  
185 as shown in Fig. 3. This work extracts and utilizes those samples located in the study area.



186

187 Figure 3. Roadside Survey (yellow: corn; green: soybean)

### 188 4. Greenest Pixel

189 NDVI is a measure of the greenness of land surface and associated objects. The values range from 0 to  
190 1. Using greenness is a great way to deal with the discontinuities between Landsat paths, in the median  
191 pixel composite due to the differences in phenology as a result of images in adjacent paths being collected

192 at different times. One way to minimize that is to set pixel values in the composite from roughly the same  
 193 phenological stage, for example, the time of maximum greenest of plants (when the leaves are on and  
 194 photosynthetically active). The entire time series is examined and the pixel with the maximum value in the  
 195 NDVI band is set as the composite value. Vegetated areas all appear green because NDVI is highest when  
 196 the vegetation in the pixel is photosynthetically active. By defining the max greenness by the maximum  
 197 NDVI, we can use the mosaic method to make a composite in which each pixel contains the maximum  
 198 NDVI pixel from the collection. The result will be the greenest pixel composite. Fig 2 shows a list of  
 199 monthly greenest pixel composite images, which are calculated for all the images captured in each month.  
 200 Indeed, compared to the median composite, the greenest pixel composite is much greener. In the greenest  
 201 images, there are fewer clouds or bad quality pixels. The images are clean and bright. In the greenest images,  
 202 the changes in crops over the time series are revealed very explicitly.

203 The re-composited, cloud-free, greenest Landsat products should be able to provide consistent spatial  
 204 and temporal comparisons of global vegetation conditions which are used to monitor the Earth's  
 205 photosynthetic vegetation activity for phenological, change detection, and biophysical interpretations. The  
 206 composites are calculated from cloud-free and atmospherically corrected gridded surface reflectance. It  
 207 requires a series of multi-temporal geo-referenced satellite data to be processed into NDVI images. Each  
 208 pixel will examine its NDVI value and only the highest value is retained for each pixel. After all the pixels  
 209 have been evaluated, the resulting image is known as the greenest image.



212 Figure 4. Monthly greenest true-color images in 2018 (top from left to right: April, May, June, July;  
 213 bottom from left to right: August, September, October, November)

214 The Landsat time-series dataset could be represented by the following definition:

215 
$$I = \{f_{y,d,lon,lat,b} \mid y \in [2013, 2019], d \in [1, 366], lon \in [-180, 180], lat \in [-90, 90], b \in [0, 11] \}$$

216 The set  $I$  represents the whole Landsat 8 dataset from 2013 to 2019. The function  $f_{y,d,lon,lat,b}$  returns  
 217 observation values.  $y$  stands for year,  $d$  is the Julian day of the year,  $lon$  and  $lat$  represent longitude and  
 218 latitude, and  $b$  means the 12 bands from the Landsat Level 1 surface reflectance products. The set of  
 219 greenest pixels is defined as:

220  $GP = \{F_{x,y,b} \mid y \in [2013, 2019], b \in [0, 11], x \in I, x' \in I, Y_x = Y_{x'}, LON_x = LON_{x'}, LAT_x = LAT_{x'}, D_x$   
 221  $\neq D_{x'}, \text{ and } NDVI_x > NDVI_{x'}\}$

222 where the  $y$  is the year,  $b$  is the bands;  $x$  and  $x'$  are two Landsat pixels; the observation year  $Y$ , latitude  
 223 ( $LAT$ ) and longitude ( $LON$ ) of  $x$  and  $x'$  are the same; the observation day  $D$  of  $x$  and  $x'$  are different; the  
 224  $NDVI$  of  $x$  is greater than the  $NDVI$  of any qualified  $x'$ . The  $NDVI$  equation is:

$$225 \quad NDVI_x = \frac{F_{x,5} - F_{x,4}}{F_{x,5} + F_{x,4}}, x \in I$$

226 For Landsat 8,  $NDVI$  is equal to the difference between band 5 and band 4 divided by the sum of the two.

## 227 5. Machine Learning Models

228 In this section, several classic ML models are introduced. They have been studied for a long time and  
 229 used in many projects. These models were tested on the GP images for comparison to find out the  
 230 algorithms with the best performance.

### 231 5.1 KNN

232 KNN, short for K nearest neighbor, is an entry-level machine learning algorithm [27]. For every pixel  
 233 in the imagery, it aims to find the K samples from the ground measurements which have the most similar  
 234 features to the pixel. In the K samples, the class with the most votes will claim the pixel.

### 235 5.2 Naïve Bayes

236 Naïve Bayes is a family of fast probabilistic algorithms and suitable for processing a large amount of  
 237 data [28]. It takes advantage of Bayes' Theorem of probability for prediction of the unknown class under  
 238 the assumption that the features have strong (naïve) independence among them. It calculates the probability  
 239 of each class for a given object, and then output the class with the highest probability. Gaussian Naïve  
 240 Bayes (Gaussian NB) extends the Naïve Bayes to real-valued attributes by assuming a gaussian distribution.  
 241 First, we can calculate the mean and standard deviation of input values ( $x$ ) for each class to summarize the  
 242 distribution. In addition to the probabilities for each class, the mean and standard deviations for each input  
 243 variable of each class must be stored as well. To make predictions, the Gaussian probability density function  
 244 (PDF) is used. The new input for the variable is plugged into the function, and in return, the gaussian PDF  
 245 will provide an estimate of the probability of that new input value for that class.

$$246 \quad PDF(x, mean, sd) = \left( \frac{1}{\sqrt{2 \times \pi} \times sd} \right) \times e^{-\frac{x - mean^2}{2 \times sd^2}}$$

247 where  $PDF(x, mean, sd)$  is the Gaussian PDF, mean and sd are the mean and standard deviation,  $\pi$  is the  
 248 numerical constant. We can then plug in the probabilities into the equation above to make predictions with  
 249 real-valued inputs [29].

### 250 5.3 AdaBoost

251 AdaBoost [30] is a classification algorithm by fitting a sequence of weak learners (models that are just  
 252 slightly better than random guessing) on repeatedly modified versions of the data. The predictions from all  
 253 of them are then combined through a weighted majority vote to get the final prediction. Each data  
 254 modification is called a boosting iteration which consists of applying weights  $w_1, w_2, \dots, w_n$  to each of the  
 255 training samples. Initially, the weights are all set to  $1/N$  ( $N$  is the total number of samples), so the first step  
 256 will simply train a weak learner on the original data. In the following steps, the weights will be individually  
 257 modified, and the learning algorithm is reapplied to the reweighted data. At each step, those incorrectly  
 258 predicted samples will have their weights increased, whereas the weights are decreased for those correctly

259 predicted. After a few iterations, samples difficult to predict will get higher and higher influence. The  
260 classifier will be forced to concentrate on the examples that are missed by the previous iterations in the  
261 sequence<sup>3</sup>.

#### 262 5.4 Random Forest

263 Random forest [31] is an improved algorithm of the basic decision tree. Instead of only one tree, the  
264 random forest will create many trees. Instead of just simply averaging the results of the trees (a forest), RF  
265 model uses two key ideas to make it random: (1) random sampling of training data points when building  
266 trees; (2) random subsets of features considered when splitting nodes. To classify a new object from an  
267 input vector, put the input vector down each of the trees in the forest. Each tree gives a classification to vote  
268 for one class. The forest chooses the classification having the most votes. When the training set for the  
269 current tree is drawn by sampling with replacement, about one-third of the cases are left out of the sample.  
270 This OOB (out-of-bag) data is used to get a running unbiased estimate of the classification error as trees  
271 are added to the forest. It is also used to get estimates of variable importance. After each tree is built, all of  
272 the data are run down the tree, and proximities are computed for each pair of cases. If two cases occupy the  
273 same terminal node, their proximity is increased by one. At the end of the run, the proximities are  
274 normalized by dividing by the number of trees. Proximities are used in replacing missing data, locating  
275 outliers, and producing illuminating low-dimensional views of the data. Because of the out-of-bag estimate  
276 internally, there is no need for cross-validation or a separate test set to get an unbiased estimate of the test  
277 set error.

278 Random forest is much better to avoid overfitting than one single decision tree. Overfitting means that  
279 the model not only learns the actual relationships in the training data, but also the noises. The noise part  
280 will make the trained model yield a very poor performance on new data.

#### 281 5.5 Support Vector Machine (SVM)

282 SVM [32] is inspired by the idea to find a hyperplane that best divides a dataset into two classes. Support  
283 vectors are the data points nearest to the hyperplane. If some support vectors are removed, the hyperplane  
284 will move too. So the support vectors are considered as the critical elements of a data set. The distance  
285 between the hyperplane and the nearest data point from either set is known as the margin. The goal is to  
286 choose a hyperplane with the greatest possible margin between the hyperplane and any point within the  
287 training set, giving a greater chance of new data being classified correctly. In other words, for linearly  
288 separable patterns, SVM could create optimal hyperplane to distinguish them. For the patterns that are not  
289 linearly separable, SVM uses the Kernel function to transform original data and map them into a new space.  
290 In that space, it would be easier to create the hyperplane.

#### 291 5.6 Multilayer Perceptron (MLP)

292 MLP [33] is one basic type of neural network which has multiple hidden layers (perceptron) beside an  
293 input layer to receive the signal and an output layer that makes decisions or predictions about the input. The  
294 arbitrary number of hidden layers that are the true computational engine of the MLP. They are trained on a  
295 strict set of input-output pairs and learn to model the correlation between the inputs and outputs. Training  
296 involves adjusting the parameters, or the weights and biases, of the model to minimize error.  
297 Backpropagation is used to make those weigh and bias adjustments relative to the error, and the error itself  
298 can be measured in a variety of ways. One usual way is by the root mean squared error.

299 MLP belongs to the family of feedforward neural networks which have two major constant activities:  
300 forward and back. In the forward pass, the signal flow moves from the input layer through the hidden layers

---

<sup>3</sup> <https://scikit-learn.org/stable/modules/ensemble.html#adaboost>

301 to the output layer, and the decision of the output layer is measured against the ground truth labels to  
302 calculate the errors. In the backward pass, using backpropagation and the chain rule of calculus, partial  
303 derivatives of the error function are back-propagated through the hidden layers. The differentiation  
304 produces a gradient along which the parameters can be adjusted to make the result of the next attempts  
305 closer to the error minimum. The forward and back processes keep going until the error is lowered under a  
306 threshold or the error doesn't change by several consecutive loops.

## 307 **6. Methods**

### 308 6.1 General description

309 This work proposed an approach to integrate the preprocessing steps of greenest pixels into the  
310 established machine learning workflow. The approach was designed to map crops including both food crops  
311 and cash crops. The training data for machine learning comes from ground-measured data and refined CDL.  
312 For the non-cropland area, the land cover labels of NLCD are assumed correct and reused in this approach.  
313 The classification is pixel-based using the multiband values of Landsat 8 as inputs and a label value as  
314 outputs. The classification module can switch among the algorithms described in Section 5.

### 315 6.2 GP-ML workflow

316 This workflow, named GP-ML, includes four main steps: 1) get greenest pixel products and identify  
317 potential crop fields; 2) assign a crop type using the CDL, roadside photos and remote sensing images; 3)  
318 perform classification using the mentioned machine learning models and the prepared training dataset; and  
319 4) refine the incorrect initial crop types in those edge areas of crop fields, and integrate the CDL product,  
320 non-crop land cover, refined ground samples, and the ML generated results to produce the final crop map  
321 products. These four steps are further described as follows.

#### 322 6.2.1 Identify Potential Crop Fields

323 To identify potential crop fields, we first compiled the areas where the Landsat imagery fully covered  
324 in the growing season and retrieve all the available images. NDVI is calculated for every Landsat image  
325 which filtered clouds and shadows based on the quality band. We extracted the pixels whose NDVI values  
326 are larger than 0.4. The threshold is set to be 0.4 based on empirical experiences and numerous experiments  
327 by referring to ground photos and samples. The pixels with NDVI larger than 0.4 have a very high chance  
328 to be at least 60% vegetation area. However, it is hard to distinguish the forests from crops simply using  
329 NDVI. We used the cultivated mask layer from USDA to further extract the pixels to get the crop fields.

#### 330 6.2.2 Image Classification

331 The greenest pixels of the recognized crop fields and the corresponding crop types are used as the  
332 training dataset for machine learning classification. The combined training data, along with all the Landsat  
333 images of 2015 are used as input data into the machine learning classifiers to train the models. The trained  
334 model will be used to produce crop maps for the next few years, e.g., 2015, 2016, 2017, 2018. During the  
335 model training, the connections between the Landsat observations and the crops growing in the fields will  
336 be learned and used to establish the rules (Random Forest, Decision Tree), create hyperplanes (SVM) and  
337 tune the weights (MLP). For the other classifiers, the encoding of crop types uses a continuous list of  
338 integers each of which represents a land cover type and all the null classes in the CDL hierarchy are cleaned.  
339 For the MLP, one-hot encoding is used to encode the crop types into arrays instead of a particular integer.  
340 The classification is mainly based on the spectral information of the pixels. Not much shape and texture  
341 information are utilized in the process. The experiments on the two sets of experimental data will reveal the  
342 benefits of greenest pixels and the better ML models for classification on greenest pixels.

#### 343 6.2.3 Accuracy assessment

344 Confusion matrix-based metrics are used to evaluate the performance of GP-ML and compare the  
345 machine learning models, evaluating its improvements over the non-GP approach. The used metrics include  
346 precision, recall, and F-1. The assessment focused on the cropland areas since the goal of the method was

347 to produce crop field maps. Two sets of sample points were selected: the first set was used to evaluate the  
 348 overall accuracy of the method to map crop fields based on greenest pixels; the second set was used to  
 349 assess the accuracy of the non-greenest pixels. To draw the first set of sample points, random sampling is  
 350 used by extracting all the areas which have NDVI values larger than 0.4. 100 points could provide a  
 351 reasonably good accuracy estimate. For each pixel, a reference point of crop types was derived by visual  
 352 interpretation from roadside photos and high-resolution images provided by USDA NAIP (National Aerial  
 353 Imagery Program).

#### 354 6.2.4 Post-refinement Processing

355 We refined the results by correcting errors such as the pixels which are classified as crops which  
 356 contrast to the ground truth and the inappropriate crop labels in the edge areas of the crop fields and the  
 357 water shallow region. The cultivated layer from USDA may exclude some crop fields or include some non-  
 358 crop fields. To correct this, we visually identified some missing fields by comparing the crop maps from  
 359 machine learning models with high-resolution satellite images. After we confirm there is a crop field, we  
 360 will manually change the mask and rerun the model to generate a crop type for the pixel. For those pixels  
 361 in wetlands or edge areas, we will determine by the neighbor pixels. If over 60% of neighbor pixels are the  
 362 same crops, we will assign the same crop type to the pixel.

### 363 7. Results

#### 364 7.1 Image Processing

365 Google Earth Engine is used to collect all the intersected Landsat scenes with the study area and 100  
 366 roadside images were processed to create 6 greenest pixel images from 2013 to 2018. The quality of the  
 367 greenest images is significantly improved and the missing pixels are much less and the cloud and shadow  
 368 areas in the original Landsat scenes are replaced or filled using the greenest observation. Jupyter notebook  
 369 is used as the developer environment. Scikit-learn library is used to train machine learning models. The  
 370 training of each model takes about 2 hours. The SVM and Random Forest takes more time than other  
 371 models. All the models are trained and tested on the same training dataset. We use the images from 2013  
 372 as the training samples and test on the images from the next five years (as shown in Table 1). Only one-  
 373 year data is used for training because we want to shorten the training time cost and emphasize the generality  
 374 test of the models. All the models are applied to both the greenest pixel and raw pixel training datasets. The  
 375 pixels are filtered by cloud and vegetation masks before they are fed into the ML models for testing. The  
 376 predicted results are ensembled back into images corresponding to their input pixel locations.

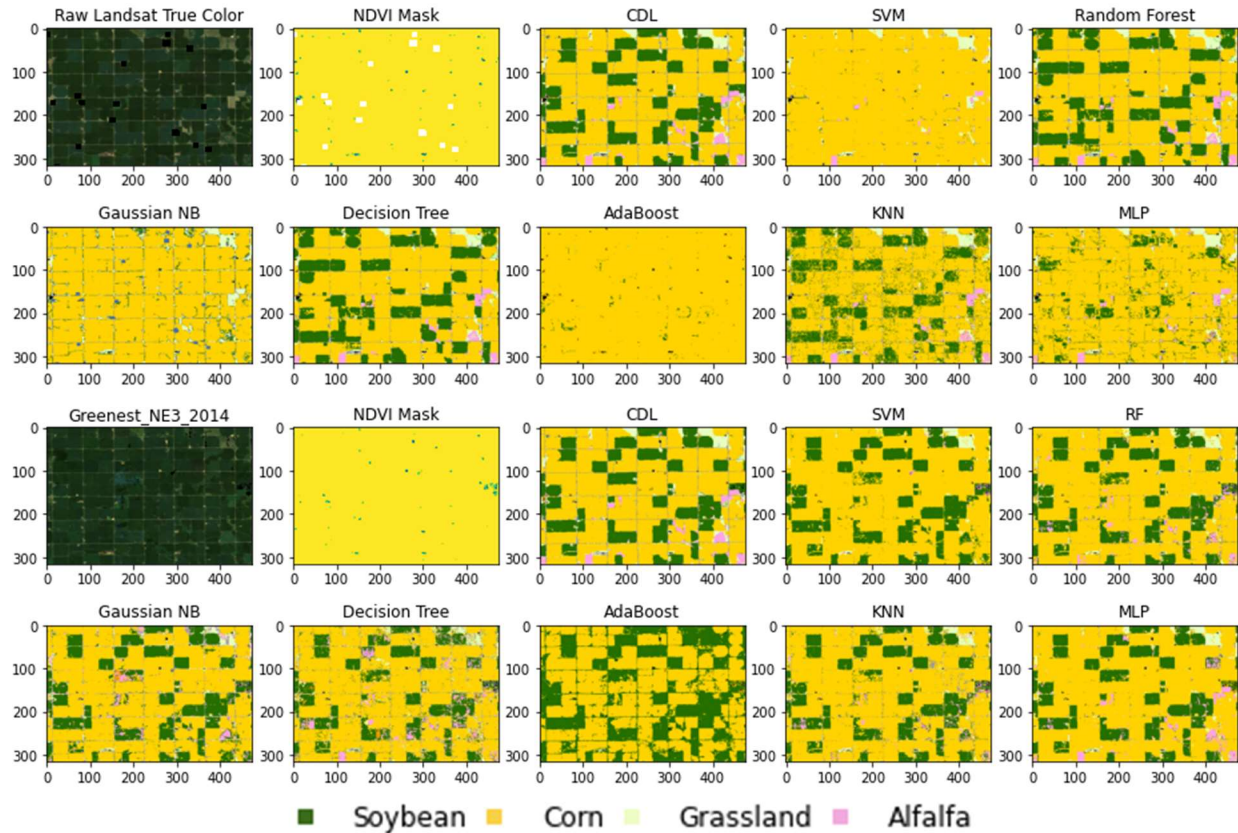
377 Table 1. Experiment Settings

Experiment	Train	Test	Methods
<b>Greenest Pixel</b>	2013 Yearly Greenest Pixels	2014 – 2018	Random Forest
			SVM
			Gaussian Naïve Bayes
			Decision Tree
			AdaBoost
			KNN
			MLP
<b>Raw Landsat Pixels</b>	2013 LC08_L1TP_031031_20130726 LC08_L1TP_031031_20130827	2014 – 2018	Random Forest
			SVM
			Gaussian Naïve Bayes
			Decision Tree
			AdaBoost
			KNN
			MLP

#### 378 7.2 Comparison of GP and non-GP

379 The results of GP and non-GP in the same year from 2014 to 2018 are compared. In Fig. 5, the top two rows show the non-GP results of Aug 14, 2014, and the bottom two rows show the GP results of 2014. The  
 380 differences are clear. In general, the GP models outperformed the non-GP models with a very large margin.  
 381

382 For the raw Landsat image, SVM and AdaBoost classified almost all the pixels to cornfields. In the  
 383 non-GP results of RF and DT, the soybean fields are misclassified to corn, while cornfields are misclassified  
 384 to soybean fields. Gaussian NB recognized most of the field edges and classify all the pixels into cornfields.  
 385 KNN generates a similar result to the Random Forest but shows some scattered soybean pixels in the middle  
 386 of cornfields. MLP result agrees with the Random Forest result on those soybean fields which are wrongly  
 387 categorized into cornfields. This experiment shows that for raw Landsat images, there is no big  
 388 improvement by only changing the classification models. The same mistaken pixels can be found in most  
 389 models' results. Overall, training data is the key to improve the accuracy and generality of the ML models.



390

391

392

393

394

395

396

397

398

399

400

401

402

403

404

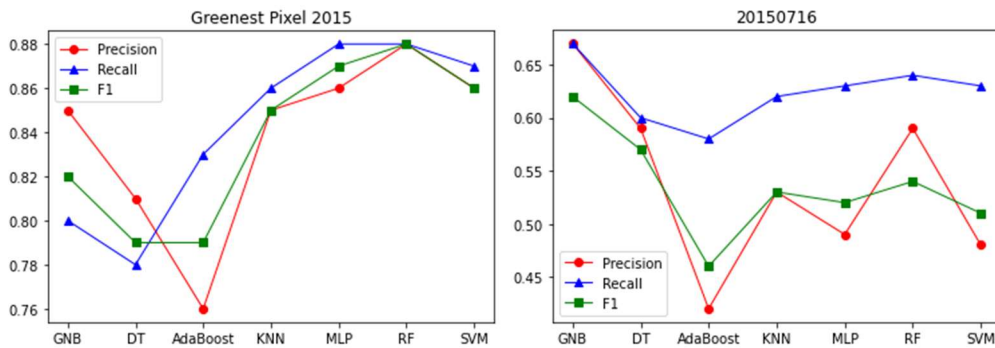
Figure 5. Comparison between 2014 non-GP (1<sup>st</sup> and 2<sup>nd</sup> rows) and 2014 GP (3<sup>rd</sup> and 4<sup>th</sup> rows) classification results (top row from left to right: true-color Landsat image, NDVI mask, CDL, SVM, Random Forest; bottom row from left to right: Gaussian NB, Decision Tree, AdaBoost, KNN, MLP)

For the greenest image, all the models generate some reasonably accurate results, with most corn and soybean fields correctly classified. The NDVI mask shows that the greenest pixel image has much fewer blank pixels than the original Landsat image. The grassland regions are greener in the true color images. The alfalfa and grassland are separated very well. The results of SVM, RF, KNN, and MLP agree on the corn and soybean fields. The difference is mainly on some scattered alfalfa pixels. From the perspective of alfalfa, the MLP result has the most identical classification to the CDL. SVM, RF, and KNN all classified some corn pixels into alfalfa. Decision Tree result has noisy texture in the cornfields with soybean pixels all over. Gaussian NB again has the best results on field edges. Gaussian NB did a good judgment, except that one small soybean field in the middle of the image is classified into alfalfa by Gaussian NB. AdaBoost

405 has the poorest prediction in this experiment. It did recognize most of the soybean and cornfields, however,  
406 neglect the short-sampled classes like grassland and alfalfa.

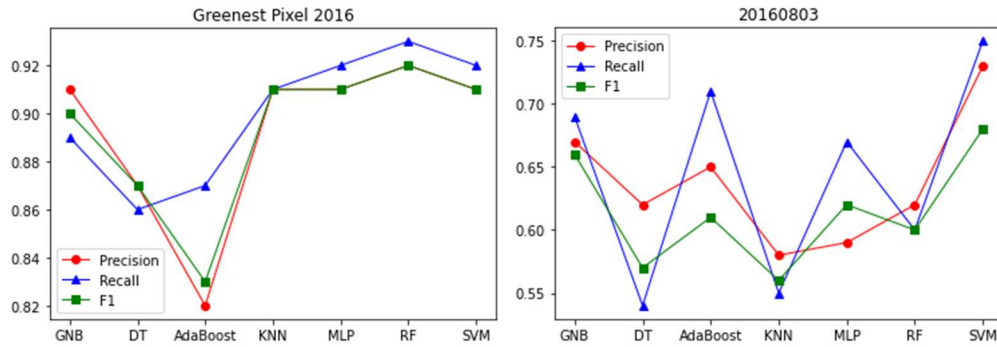
407 After observing the two experiments, it is clear that every ML model did a better prediction on the  
408 greenest pixel image than the raw Landsat image. It proves the quality of the training data plays a key role  
409 in crop classification. The conclusion could be supported by quantitative metrics of accuracy. The measures  
410 of both experiments on the test datasets of four years (2015-2018) are plotted in Fig. 6. Three common  
411 indicators are evaluated against the result pixels and the ground truth. The precision of the same models is  
412 higher than 76% on GP but less than 70% on non-GP in 2015. In the 2015 GP experiment, RF has the most  
413 consistent accuracy with the second-highest precision (only after MLP) and the highest recall and F1 score  
414 (88%). In the non-GP experiment on the Landsat image of July 16, 2015, Gaussian NB is the most accurate  
415 model on all three metrics. In the 2016 results, the GP-based RF achieves as high as 92% in precision and  
416 94% in recall. KNN, MLP, and SVM also did very well on precision and recall. Decision and AdaBoost  
417 are not as good as the other four. However, on the non-GP, SVM performs the best with 72% precision,  
418 75% recall, and 67% F1. KNN has the lowest precision and F1 and Decision Tree has the lowest recall. In  
419 the 2017 result, GP-trained SVM outperforms the other methods with a very consistent value (89%) on the  
420 three indicators. The decision tree is the model with the worst result. For the non-GP in 2017, AdaBoost  
421 has the best performance with 74% precision, 79% recall, and 74% F1, and KNN has the poorest measures.  
422 In the 2018 GP result, RF again claims the first place with 90% precision, 90% F1 and 93% recall. MLP  
423 and SVM did the same best. DT and AdaBoost are the two models with the worse predictions. In the non-  
424 GP 2018 result, Gaussian NB is the best model and the AdaBoost is the worst.

425 The experiment results show that the models have very unstable performances on the non-GP data. It  
426 is found to be very inconsistent over the four years on the best and worst models. In every year, the non-  
427 GP-trained models perform very poorly (50% ~ 75% in precision) on new data (trained on 2013 and tested  
428 on the subsequent years), which reflects the generality of the trained models is bad. However, the same  
429 models trained on GP have very solid and relatively steady accuracy (about 80% ~ 95%). The model  
430 performs better on GP than non-GP in every case. The results have the most consistent precision and recall.  
431 The two metrics differ dramatically in the non-GP results, which indicates that the non-GP-trained models  
432 either underfit on the majority or overfit on the minority. In conclusion, the GP training dataset could  
433 significantly improve the accuracy of the result crop maps on both major crops and minor crops. The models  
434 trained on GP have much better generality and accuracy than those trained on non-GP.

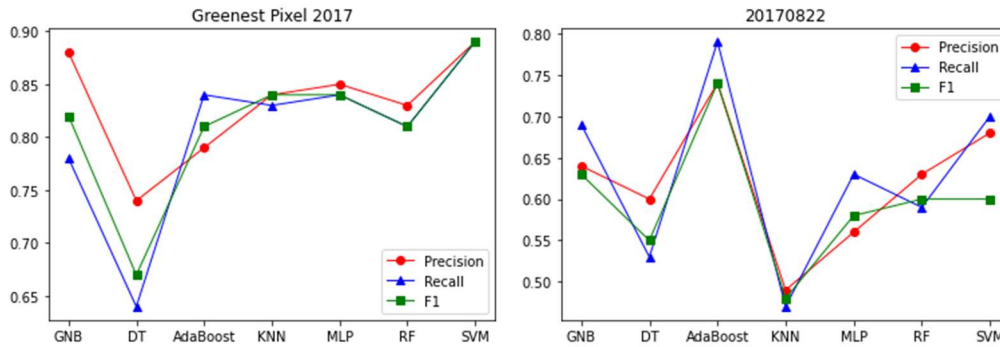


435

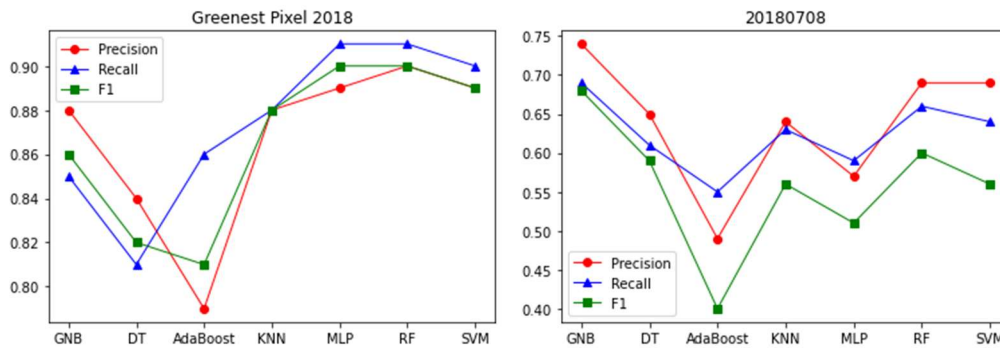
436



437



438



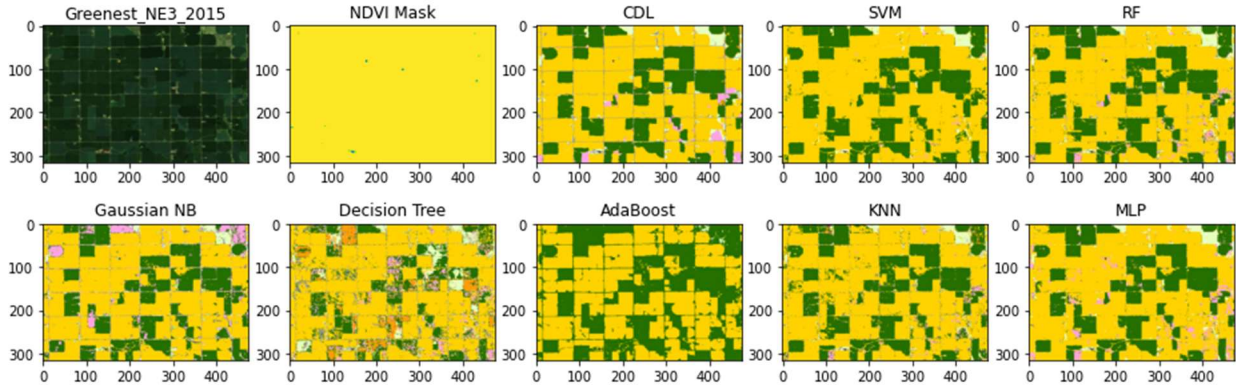
439 Figure 6. Accuracy Comparison of ML models on greenest pixels (left) and raw Landsat pixels (right)

440 7.3 Comparison of ML Algorithms

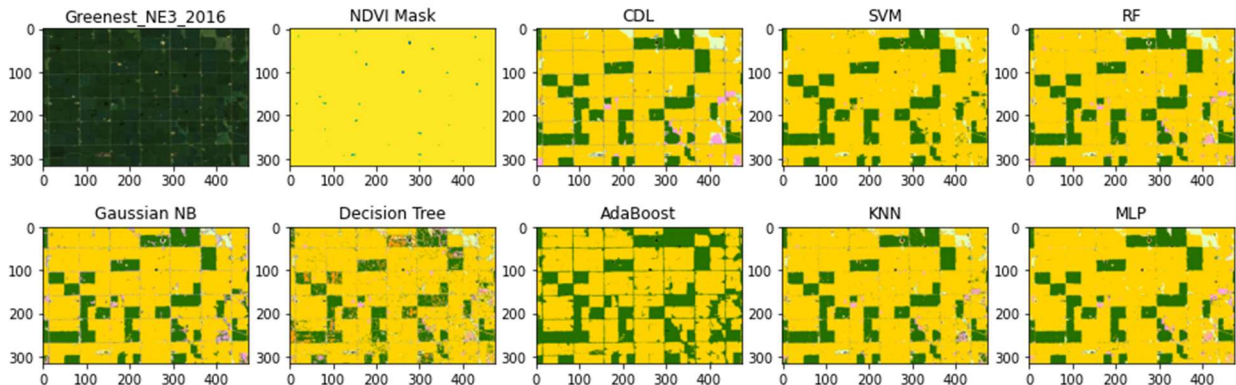
441 To find the best algorithm for GP, the results of the GP-trained models in all four years (as shown in  
 442 Fig. 7) are thoroughly studied. Every year, the ML models display a similar pattern in their judgments.  
 443 SVM can accurately identify soybeans, corns, and grassland, but cannot recognize alfalfa and field edges.  
 444 SVM misclassified most alfalfa pixels into soybeans. Gaussian NB makes big mistakes in some big soybean  
 445 fields by classifying them into alfalfa fields. Corn and grasslands are correct. The results of single Decision  
 446 Tree are very poor with vague and dirty texture and many pixels with classes that don't exist in the region.  
 447 Single Decision Tree is not recommended for this purpose. AdaBoost did a good job of outlining the field  
 448 borders. It made the right judgment on the major crops but completely ignored the minor crops. The pixels  
 449 of grassland and alfalfa are assigned to either corn or soybeans (mostly). KNN outputs a very similar result  
 450 to the RF and MLP, except for some error spots of soybeans in the middle of cornfields. The KNN result is  
 451 less smooth and consistent compared to RF and MLP.

452 The results of RF and MLP are better than other models. models accurately recognize the soybean, corn  
 453 and grassland fields. It is hard to tell which one of the two is the best. RF delineates the field borders more  
 454 clearly than MLP while MLP gives better prediction on alfalfa than RF. In other words, if the borders are  
 455 important target information, RF is recommended; if minor crops like alfalfa are required information, MLP  
 456 would be the better choice.

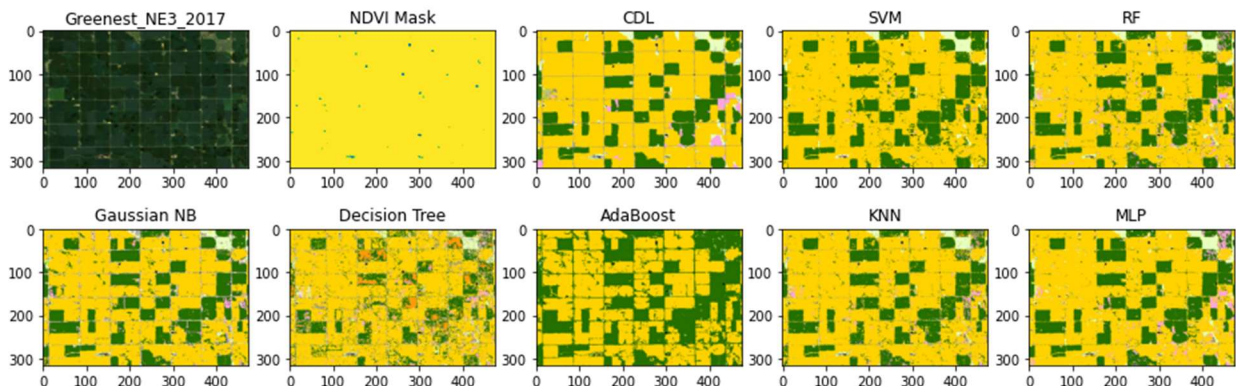
457



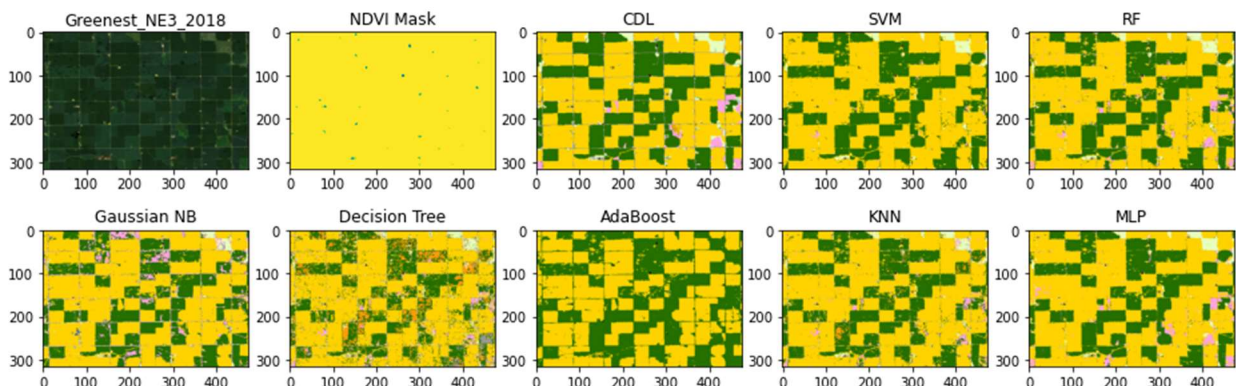
458



459



460



■ Soybean ■ Corn ■ Grassland ■ Alfalfa

461

462

463

Figure 7. Comparison of the Algorithms on greenest pixels (trained on 2015, tested on 2013, 2014, 2016, 2017, 2018)

464 **8. Discussion**

465 8.1 **Reliability:** will the GP-trained models always beat the non-GP models?

466 Based on the experiment results, the GP-trained ML models outperformed the non-GP-trained models.  
467 To rule out the concerns on coincidences, we did another test in the region shown in Fig. 1 and got the same  
468 results (GP better than non-GP). The reason is that in the GP the crops and non-crop vegetation are all in  
469 their greenest phases, which narrows down the characteristics of the crops into a limited feature space.  
470 Therefore, using the GP training dataset the ML models don't need to make wild guesses on which phase  
471 the crops are in and require fewer rules or features to distinguish the crops. In other words, the GP training  
472 dataset makes the job of ML models much easier than the non-GP training dataset. The superiority of GP-  
473 trained models over non-GP models is not coincidental and should be reproducible all the time.

474 8.2 **Generality:** will the best ML models for this region always be the top choice for any other regions?

475 The comparison of ML models in image classification has been studied for a very long time. As one of  
476 the common techniques for improvements, hyperparameter tuning could greatly alter the performance of  
477 the ML models and bring a lot of uncertainties to the comparison. In this study, we didn't do much tuning  
478 on the hyperparameters. All the parameters use their default values provided by the ML library. If the  
479 hyperparameter tuning is taken into consideration, the answer to the generality question would be a NO.  
480 However, if taking hyperparameter tuning off the table, the answer would be certainly a YES. Without  
481 tuning parameters, the Random Forest and Multilayer Perceptron will produce better results for all the  
482 regions out of the six listed ML models.

483 8.3 **Scalability:** will the same quality results be achieved if the region is extended to a larger scale?

484 This question needs more experiments on bigger datasets to answer. At this point, we could only  
485 anticipate from the theoretic perspective. The quality of training data would still be key to scale the trained  
486 models to be applied in a larger scope. If the samples used for training are less biased and cover most of the  
487 unique statuses of the objects, the trained model would obtain more capability to deal with the upcoming  
488 new pixels from new images of various regions. The bias of training data is not only about the regions, but  
489 also in the classes. Naturally, some crops have more samples (e.g., corn and soybean) while others have  
490 fewer occurrences (e.g., lentils). Each class should have a certain minimum number of samples in the  
491 training data to ensure the minority crops could be distinguished. In the GP approach, the variety of regions  
492 have relatively fewer impacts on the results as the same crop of different regions has very similar spectral  
493 characteristics during its greenest stage (assuming the climate of those regions is similar). Overall, better  
494 scalability will be achieved with better training data.

495 **9. Conclusion**

496 This paper proposes a novel approach using greenest images and ML algorithms in producing crop  
497 maps. Greenest images are calculated by extracting the greenest pixel value from all the captured images  
498 in one year. The greenness is measured by NDVI (normalized difference vegetation index). The pixels with  
499 the highest NDVI values are considered as the greenest pixels. The pixels in the greenest image should all  
500 be the greenest. An approach is created to generate and take the greenest images as inputs and output a  
501 semantic map of crop types. The map is a raster image, in which the pixel values correspond to crop  
502 categories. A new workflow streamlining the preparation and feeding of greenest images into ML models  
503 is built and experimented. The workflow will translate the ML model results in crop maps which are ready  
504 for stakeholders to use. The whole workflow involves dozens of tools, resources, and libraries, and requires  
505 better management to improve efficiency. The study area chooses a farm located in the heart of Nebraska  
506 and the data sources are Landsat and USDA NASS CDL. The images are preprocessed to become  
507 consumable arrays in ML models. The training among the hidden layers of ML models will extract the  
508 high-level features to identify and recognize the crops. RF and MLP have been proven to be more accurate

509 and robust than the other classification models. The trained model is supposed to be reusable on future  
510 images to automatically generate crop maps without needs for collecting new ground truth or retraining.  
511 The results show that the GP-trained ML models outperformed the non-GP-trained ML models with a very  
512 large margin.

513 In the future, more experiments on a bigger training dataset will be conducted to verify the superiority  
514 of the GP-based approach in larger regions. More advanced ML models such as convolutional neural  
515 networks and recurrent neural networks will be tested against GP to further improve the accuracy. The  
516 readiness of the GP-trained model to produce official crop maps from remote sensing images will be  
517 evaluated and carried out in Nebraska in our next step of research.

518

## 519 Reference

520

- 521 1. Sun, Z.; Di, L.; Fang, H. Using long short-term memory recurrent neural network in land cover  
522 classification on Landsat and Cropland data layer time series. *International Journal of Remote*  
523 *Sensing* **2018**, *40*, 593-614.
- 524 2. Pinter Jr, P.J.; Hatfield, J.L.; Schepers, J.S.; Barnes, E.M.; Moran, M.S.; Daughtry, C.S.; Upchurch,  
525 D.R. Remote sensing for crop management. *Photogrammetric Engineering & Remote Sensing*  
526 **2003**, *69*, 647-664.
- 527 3. Adão, T.; Hruška, J.; Pádua, L.; Bessa, J.; Peres, E.; Morais, R.; Sousa, J. Hyperspectral imaging: A  
528 review on UAV-based sensors, data processing and applications for agriculture and forestry.  
529 *Remote Sensing* **2017**, *9*, 1110.
- 530 4. Sun, J.; Di, L.; Sun, Z.; Shen, Y.; Lai, Z. County-Level Soybean Yield Prediction Using Deep CNN-  
531 LSTM Model. *Sensors* **2019**, *19*, 4363.
- 532 5. Sun, Z.; Di, L.; Fang, H.; Burgess, A.B.; Singh, N. Deep Learning Cyberinfrastructure for Crop  
533 Semantic Segmentation. In Proceedings of AGU Fall Meeting 2019.
- 534 6. Sun, Z. Automatically Recognize Crops from Landsat by U-Net, Keras and Tensorflow. Availabe  
535 online: [https://medium.com/artificial-intelligence-in-geoscience/automatically-recognize-crops-](https://medium.com/artificial-intelligence-in-geoscience/automatically-recognize-crops-from-landsat-by-u-net-keras-and-tensorflow-7c5f4f666231)  
536 [from-landsat-by-u-net-keras-and-tensorflow-7c5f4f666231](https://medium.com/artificial-intelligence-in-geoscience/automatically-recognize-crops-from-landsat-by-u-net-keras-and-tensorflow-7c5f4f666231) (accessed on 1/26/2020).
- 537 7. Zhong, S.; Xu, Z.; Sun, Z.; Yu, E.; Guo, L.; Di, L. Global vegetative drought trend and variability  
538 analysis from long-term remotely sensed data. In Proceedings of 2019 8th International  
539 Conference on Agro-Geoinformatics (Agro-Geoinformatics); pp. 1-6.
- 540 8. Sun, Z.; Di, L.; Zhang, C.; Fang, H.; Yu, E.; Lin, L.; Tan, X.; Guo, L.; Chen, Z.; Yue, P. Establish  
541 cyberinfrastructure to facilitate agricultural drought monitoring. In Proceedings of Agro-  
542 Geoinformatics, 2017 6th International Conference on; pp. 1-4.
- 543 9. Sun, Z.; Di, L.; Zhang, C.; Fang, H.; Yu, E.; Lin, L.; Tang, J.; Tan, X.; Liu, Z.; Jiang, L. Building robust  
544 geospatial web services for agricultural information extraction and sharing. In Proceedings of  
545 Agro-Geoinformatics, 2017 6th International Conference on; pp. 1-4.
- 546 10. Sun, Z.; Peng, C.; Deng, M.; Chen, A.; Yue, P.; Fang, H.; Di, L. Automation of Customized and  
547 Near-Real-Time Vegetation Condition Index Generation Through Cyberinfrastructure-Based  
548 Geoprocessing Workflows. *Selected Topics in Applied Earth Observations and Remote Sensing,*  
549 *IEEE Journal of* **2014**, *7*, 4512-4522, doi:10.1109/jstars.2014.2377248.
- 550 11. Yang, Z.; Di, L.; Yu, G.; Chen, Z. Vegetation condition indices for crop vegetation condition  
551 monitoring. In Proceedings of Geoscience and Remote Sensing Symposium (IGARSS), 2011 IEEE  
552 International; pp. 3534-3537.

- 553 12. Xiong, J.; Thenkabail, P.S.; Gumma, M.K.; Teluguntla, P.; Poehnelt, J.; Congalton, R.G.; Yadav, K.;  
554 Thau, D. Automated cropland mapping of continental Africa using Google Earth Engine cloud  
555 computing. *ISPRS Journal of Photogrammetry and Remote Sensing* **2017**, *126*, 225-244.
- 556 13. Moran, M.S.; Inoue, Y.; Barnes, E. Opportunities and limitations for image-based remote sensing  
557 in precision crop management. *Remote Sensing of Environment* **1997**, *61*, 319-346.
- 558 14. Banman, C. Supervised and Unsupervised Land Use Classification. Available online:  
559 <http://academic.emporia.edu/aberjame/student/banman5/perry3.html> (accessed on  
560 15. Sun, Z.; Fang, H.; Di, L.; Yue, P.; Tan, X.; Bai, Y. Developing a web-based system for supervised  
561 classification of remote sensing images. *GeoInformatica* **2016**, 1-21.
- 562 16. Johnson, D.M.; Mueller, R. The 2009 cropland data layer. *Photogramm. Eng. Remote Sens* **2010**,  
563 *76*, 1201-1205.
- 564 17. Boryan, C.; Yang, Z.; Mueller, R.; Craig, M. Monitoring US agriculture: the US department of  
565 agriculture, national agricultural statistics service, cropland data layer program. *Geocarto*  
566 *International* **2011**, *26*, 341-358.
- 567 18. Quinlan, J.R. See5. URL: <http://www.rulequest.com/see5-info.html> **1997**.
- 568 19. Duro, D.C.; Franklin, S.E.; Dubé, M.G. A comparison of pixel-based and object-based image  
569 analysis with selected machine learning algorithms for the classification of agricultural  
570 landscapes using SPOT-5 HRG imagery. *Remote Sensing of Environment* **2012**, *118*, 259-272,  
571 doi:<http://dx.doi.org/10.1016/j.rse.2011.11.020>.
- 572 20. Waldner, F.; Canto, G.S.; Defourny, P. Automated annual cropland mapping using knowledge-  
573 based temporal features. *ISPRS Journal of Photogrammetry and Remote Sensing* **2015**, *110*, 1-  
574 13.
- 575 21. Fritz, S.; See, L.; McCallum, I.; You, L.; Bun, A.; Moltchanova, E.; Duerauer, M.; Albrecht, F.; Schill,  
576 C.; Perger, C. Mapping global cropland and field size. *Global change biology* **2015**, *21*, 1980-  
577 1992.
- 578 22. Gao, F.; Anderson, M.C.; Zhang, X.; Yang, Z.; Alfieri, J.G.; Kustas, W.P.; Mueller, R.; Johnson,  
579 D.M.; Prueger, J.H. Toward mapping crop progress at field scales through fusion of Landsat and  
580 MODIS imagery. *Remote Sensing of Environment* **2017**, *188*, 9-25.
- 581 23. Roy, D.P.; Wulder, M.; Loveland, T.; Woodcock, C.; Allen, R.; Anderson, M.; Helder, D.; Irons, J.;  
582 Johnson, D.; Kennedy, R. Landsat-8: Science and product vision for terrestrial global change  
583 research. *Remote Sensing of Environment* **2014**, *145*, 154-172.
- 584 24. EOS. NDVI FAQ: All You Need to Know About NDVI. Available online: <https://eos.com/blog/ndvi-faq-all-you-need-to-know-about-ndvi/> (accessed on 2020.03.16).
- 585 25. Johnson, G.L.; Haver, C.B. Decision-making principles in farm management. **1953**.
- 586 26. USDA, F. Common land unit. *FSA Handbook, 8-CM* **1998**.
- 587 27. Dudani, S.A. The distance-weighted k-nearest-neighbor rule. *IEEE Transactions on Systems, Man,  
588 and Cybernetics* **1976**, 325-327.
- 590 28. Chan, T.F.; Golub, G.H.; LeVeque, R.J. Updating formulae and a pairwise algorithm for computing  
591 sample variances. In Proceedings of COMPSTAT 1982 5th Symposium held at Toulouse 1982; pp.  
592 30-41.
- 593 29. Brownlee, J. Naive Bayes for Machine Learning. Available online:  
594 <https://machinelearningmastery.com/naive-bayes-for-machine-learning/> (accessed on  
595 4.13.2020).
- 596 30. Hastie, T.; Rosset, S.; Zhu, J.; Zou, H. Multi-class adaboost. *Statistics and its Interface* **2009**, *2*,  
597 349-360.
- 598 31. Breiman, L. Random forests. *Machine learning* **2001**, *45*, 5-32.
- 599 32. Cortes, C.; Vapnik, V. Support-vector networks. *Machine learning* **1995**, *20*, 273-297.

- 600 33. SUTER, B.W. The multilayer perceptron as an approximation to a Bayes optimal discriminant  
601 function. *IEEE Transactions on Neural Networks* **1990**, *1*, 291.  
602